Isomechanical Groups in Molecular Crystals and Role of Aromatic Interactions

DOI:
10.1021/acs.cgd.0c01188

Document Version
Accepted author manuscript

Isomechanical Groups in Molecular Crystals and Role of Aromatic Interactions

Benjamin P. A. Gabriele[a], Craig J. Williams[b], Matthias Eckhard Lauer[c], Brian Derby[b], Aurora J. Cruz-Cabeza[a]*

[a] Department of Chemical Engineering and Analytical Science, University of Manchester, UK.
[b] Department of Materials, University of Manchester, UK.
[c] Roche Innovation Center Basel, Basel, Switzerland

*Email: aurora.cruzcabeza@manchester.ac.uk

Abstract

We have measured mechanical properties in molecular crystals of a series of *para*-substituted benzoic acids using nanoindentation. Two linear correlations were found for these materials: first between the Young's modulus and the melting point per unit of volume, and second between the hardness and the crystal cohesive energy density. These correlations, however, were found to only hold within *isomechanical groups*. These are groups of materials with similar interaction strengths and dimensionalities. A close analysis of the intermolecular interactions presents in these crystals revealed that structures with aromatic rings interacting through t-type interactions may achieve higher interaction dimensionalities and thus result in harder crystals than those with rings interacting through aromatic stacking. In these systems, thus, the dimensionality of the aromatic interactions in the crystals appears to play the major role in their mechanical behaviour.

Key words: nanoindentation, molecular crystals, isomechanical groups

1. Introduction

Small molecule drug discovery delivers series of novel chemical entities, which achieve good potency at low toxicity. The development of a novel drug candidate into a medicine for oral delivery requires the development of a pharmaceutical formulation, to ensure constant and defined dosing in therapies. The physicochemical properties of novel candidates are, at stages of early drug discovery, unknown. Central material properties, such as crystal polymorphism or the solubility in intestinal fluids, can only be discovered at later stages, even though they define the oral bioavailability from a general point of view and material properties constrain the design space of the pharmacists. Therefore, the design of formulation and manufacturing processes profits from an early and insightful knowledge of structure-property relation: in that sense, mechanical properties are particularly important because the pharmaceutical active ingredients (APIs) need to be crystallised, ground, blended and compacted into a tablet with sufficient shelf-live stability. Being able to accurately measure and even predict mechanical properties in molecular crystals is thus, very desirable from a formulation perspective.[1]

The properties of solid materials are controlled by the nature of their interatomic and intermolecular forces (bonding) and, for crystalline materials, also by their short and long-range arrangement (structure) as well as their impurity profile and defects. This was first investigated for a range of polymers by Beaman who explored correlations between physical properties.[2] Brown and Ashby[3] examined the relationship between the physical properties of materials with a range of crystal structures and chemistries and proposed that many of these

physical properties were scaled by the materials melting temperature, T_M. This observation was further developed by Ashby and co-workers to argue that materials with similar structure and type of bonding can be collected into a common grouping or "material class", whose members have materials properties that are similar and characteristic of their class.[4,5] These material classes, sometimes called *isomechanical groups* because of their strong correlations in mechanical properties, can have their properties conveniently expressed using characteristic constants such as melting temperature and physical density. These correlations are strongest for properties, such as elastic constants, which are closely related to crystal structure and bonding strength but can also be useful for defect dominated properties such as strength, hardness and toughness. Frost and Ashby[6] reported a strong correlation between Young's modulus, E, and a material's melting temperature expressed using the following dimensionless relation:

$$E = A\left(\frac{k_B T_M}{\Omega}\right) \quad \textbf{(1)}$$

where Ω is the atomic volume of the material, k_B is the Boltzmann's constant and A is a numerical constant. The numerical constant, A, may vary as a function of the crystal structure and bond type within a class of materials and, from their compilation of data encompassing a large range of metals and ceramics, they suggested that $A \approx 100$. Other studies confirmed that such a correlation was appropriate for geological materials[7] and semiconductors.[8] In addition Plummer and Todd[9] found that correlations could also be applied to metallic glasses, using the glass transition temperature (T_g) instead of the melting point.

However, to the best of our knowledge, no equivalent correlations have been established for molecular crystals. Roberts and Rowe compared the hardness data of molecular single crystals[10] and found a correlation between hardness and cohesive energy density (CED), or lattice energy per unit of volume. They also compared the CED of a series of molecular powders with their Young's modulus with a certain success[11] but did not use Ashby's scaling law or include the melting point in the correlation.

Here we study the mechanical properties of single crystals of seven benzoic acid derivatives (Figure 1), selected as model materials for various reasons. First, they are easy to crystallise as single crystals. Second, they have physical and chemical similarities to compounds of pharmaceutical interest. Third, they have comparable mean molecular volumes Ω (same order of magnitude) and are rather simple molecules due to their small size as compared to commercial APIs. These compounds differ in the substituent located at the para position from the aromatic carboxylic acid. The compounds studied and their crystal structures are: Benzoic Acid (BA, CSD refcode: BENZAC02[12]), *p*-toluic acid (*p*TA, CSD refcode: PTOLIC[13]), *p*-aminobenzoic acid form α (*p*ABA, CSD refcode: AMBNAC06[14]), *p*-nitrobenzoic acid form II (*p*NBA, CSD refcode: NBZOAC14[15]), *p*-bromobenzoic acid (*p*BrBA, CSD refcode: BRBZAP[16]), *p*-iodocenzoic acid (*p*IBA, CSD Refcode: BENMOW01[17]) and *p*-butoxybenzoic acid (*p*BOBA, CSD refcode: BUXBZA02[18]). We have first divided the compounds in two groups determined by their crystal system, respectively monoclinic and triclinic, as identified in Figure 1.

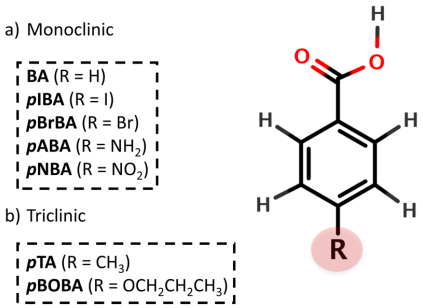

Figure 1. Benzoic acid derivatives studied in this work.

Since mechanical properties of the materials selected are not readily available in the published literature, we have first used nanoindentation[19,20] to determine their elastic modulus and hardness to then assess the applicability of Frost and Ashby's correlation (Equation 1) to molecular crystals and reassessed a possible correlation between hardness and cohesive energy density for molecular crystals.

Nanoindentation allows the assessment of elastic and plastic properties of small volumes of materials requiring only a few single crystals. Although the technique is routinely used to characterise hard inorganic materials (i.e. metals and ceramics), it has only recently been used to study molecular crystals.[21–23] However there are significant experimental challenges that arise when using nanoindentation on molecular crystals. For example, it is often difficult to grow large, good quality single crystals suitable for nanoindentation of complex organic compounds. A further point to note with nanoindentation concerns the analysis of the load/displacement trace to determine the elastic properties of the material being tested. The analysis initially developed by Oliver and Pharr,[19,20] and now incorporated in the International Standard ISO 14577,[24] returns the reduced elastic modulus, E_R, which is defined as:

$$E_R = \frac{E}{1 - \upsilon^2} \qquad \textbf{(2)}$$

where E is Young's modulus and ν is Poisson's ratio. In addition, the analysis assumes that the material is an isotropic solid, whereas its use with molecular crystals should take into account crystal anisotropy. Previous studies with sucrose,[25] saccharin,[21] aspirin[26] and α-glycine[27] have found that the indentation derived elastic modulus returns results that depend on the crystal face chosen for the experiment.

2. Methods

Crystallisation. Single crystals of benzoic acid (>99.5%, ACS reagent, Sigma-Aldrich) and *p*-aminobenzoic acid form α (99%, Acros Organicos) were obtained from two independent slow cooling crystallisation conditions: i) for benzoic acid, freshly distilled and deionised water (23MΩ.cm at 25°C when the solution was prepared) was cooled from 50 to 25 °C with a concentration corresponding to a supersaturation ratio $S = C_{solution}/C_{solubility} = 1.6$ at the final temperature ii) for *p*-aminobenzoic acid form α, acetonitrile (> 99.9%, HPLC grade, Fisher Chemical) from 45 to 20 °C with a concentration corresponding to a supersaturation ratio of S = 1.3 at the final temperature. Cooling rate was -1 °C/hr in both cases.

p-Toluic acid (98%, Acros Organicos), *p*-bromobenzoic acid (98%, Aldrich Chemistry) and *p*-iodobenzoic acid (98%, Aldrich Chemistry) crystals were all produced by the slow evaporation at room temperature of their respective saturated isopropanol (puriss. > 99.5%, Merck) solution. *p*-nitrobenzoic acid form II (>98%, Fluka Analytical) crystals were produced by the slow evaporation at 70 °C of a saturated acetonitrile (> 99.9%, HPLC grade, Fisher Chemical) solution. *p*-Butoxybenzoic acid single crystals were obtained from slow evaporation from a saturated toluene (anhydrous, 99.8%, Sigma-Aldrich) solution with commercial powder of *p*BOBA (98%, Fluorochem). For BA, *p*TA, *p*NBA, *p*BrBA and *p*IBA, when crystals appeared larger than c.a. 250-500 μm, the solutions were filtered using a Buchner funnel, and crystals were quickly recovered and consequently handled with tweezers or spatula only. In parallel, large and thick crystals (c.a 1 to 3 mm thickness) of *p*ABA and *p*BOBA were produced. Crystals were large enough to be recovered using tweezers and dried on a clean tissue paper. All measurements were made within 3 days of harvesting the crystals.

DSC. Melting points were assessed via Differential Scanning Calorimetry (DSC, DSC2500, TA Instruments). Single crystals obtained from the methods described above were used for the analyses. Between 3 and 8 single crystals, depending on the crystals size, were placed into DSC pans (Tzero Pan T181128, TA Instruments). Three independent measurements were made per compound, with one unique heating cycle per measurement from 30 °C up to 150 – 300 °C depending on the expected melting point, with a heating rate of 10°C/min.

Face indexing. Representative single crystals of the compounds studied were face indexed at room temperature using a single crystal x-ray diffractometer (XCalibur-2, Oxford) equipped with a MoKα X-ray source (λ = 0.71073Å). The Miller indices used here refer to the unit cell parameters defined by the CSD refcodes BENZAC02[12], PTOLIC[13], AMBNAC06[14], NBZOAC14[15], BRBZAP[16], BENMOW01[17] and BUXBZA02[18] for BA, *p*TA, *p*ABA form α, *p*NBA form II, *p*BrBA, *p*IBA and *p*BOBA respectively. From the X-ray measurements, the unit cells of each single crystal were first verified to match the CSD refcode associated. Indexing of the faces was carried out with the software CrysAlisPro[28] (version 171.40.14d, Rigaku Oxford Diffraction).

Nanoindentation. Experiments were carried out on 7 to 10 single crystals per molecule studied (9 indents per crystal) using a Hysitron Ti950 Triboindenter (Hysitron/Bruker) equipped with a diamond Berkovich probe. Indents were carried out on selected single crystals whose crystal shape clearly matched that identified during face indexing. Crystals of BA, *p*BrBA and *p*IBA were cleaved using adhesive tape to reveal a smooth surface free of environmental contamination, however this simple cleavage technique was not successful with the crystals of other compounds. In those cases, the crystals were indented as harvested without further treatment. Indentations were conducted in either load-control or displacement-control mode using a trapezoid load function. The distance between individual indents was set to 25 μm. Reduced modulus and hardness were extracted from the indentation curves as stated in ISO 14577 using a PS-1 sheet calibration sample (E_R = 2.91 GPa, VPG Micro-measurements, Malvern, USA). This calibration sample was indented in between each series of indents, i.e. in-between each single crystal tested, in an attempt to assess and monitor possible tip contamination. We first investigated the optimal maximum displacement/load as defined in previous work, so the modulus and hardness measured do not vary for further increase of decrease of P_{MAX} or h_{MAX}.[29] Crystals of BA and *p*NBA form II were indented in

displacement-controlled mode, with a 5 second loading time, 2 second holding time and 5 second unloading time, with a set maximum displacement used h_{MAX} = 425 nm. The other crystals were all indented in load-controlled mode, with a 5 second loading time and a 5 second unloading time. Holding time was set to 2 seconds for *p*TA and to 5 seconds for *p*ABA, *p*BrBA and *p*IBA in order for the indenter depth to stabilise at P_{MAX} and to reduce viscous effects. P_{MAX} was set to 3 mN for *p*TA, *p*BrBA and *p*IBA, and 5mN for *p*ABA.

Imaging. Crossed polarised light was used to identify single crystals of good quality using an Axioplan2 Zeiss Microscope in transmission mode. For each compound, height map images were recorded after some indentation events by contact mode in-situ scanning probe microscopy (SPM) using the Berkovich probe used for indentation, and by atomic force microscopy (AFM, Multimode 8, Bruker) using PeakForce QNM in Air mode with a TESP-V2 probe (k = 42 N/m).

Calculation of lattice energies and Periodic Bond Chains. Lattice energies (U_{Latt}) of the crystal structures retrieved from the CSD were calculated using Material Studio 2019 (Dassault Systèmes, BIOVIA)[30] with the COMPASSII forcefield (and its atomic charges). Crystal structures were geometry optimised by relaxing all atomic positions in the unit cell while keeping the unit cell parameters constant to the experimental values which were all collected at room temperature. Energies of the relaxed unit cells were then normalised by the number of molecules in the unit-cell ($U_{CRYSTAL}$). In a separate simulation, a single molecule of the compound of interest was fully optimised in the gas phase using the same energy model (U_{GAS}). The lattice energy U_{LATT} was then calculated for each compound as $U_{LATT} = U_{CRYSTAL} - U_{GAS}$. Periodic Bond Chains (PBCs) were generated using the same energy model and a cut off of -13 kJ/mol for visualisation. PBCs were generated by computing molecule-molecule interactions of a central molecule with its neighbours. These molecule-molecule energies were then used to generate an interaction network, or PBCs, within a larger supercell.

3. Face indexing and crystal packing

BA, *p*ABA form α, *p*NBA form II, *p*BrBA and *p*IBA crystallise in the monoclinic system, with space groups $P2_1/c$, $P2_1/n$, $P2_1/c$, $P2_1/a$ and $P2_1/a$, respectively. *p*TA and *p*BOBA by contrast crystallise in the triclinic system, with the P-1 space group. Beyond their crystal system, another way to classify this series of crystals is by identifying the bonding environment within the crystal packing. All the 7 molecules are involved in both hydrogen-bonding and aromatic interactions.

All seven compounds form strongly bonded dimers through $R^2_2(8)$ hydrogen bonds between two -COOH groups (Figure 2, arrow 1). This interaction is 0-dimensional, since it does not extend beyond the dimer itself, and its impact towards mechanical resistance is likely to be negligible. Compounds are also involved in aromatic interactions of two types: aromatic stacks (observed in BA, *p*ABA form α, *p*NBA form II, *p*BrBA, *p*IBA and *p*TA, Figure 2a) and t-type interactions (observed in *p*BOBA, triclinic, Figure 2b).

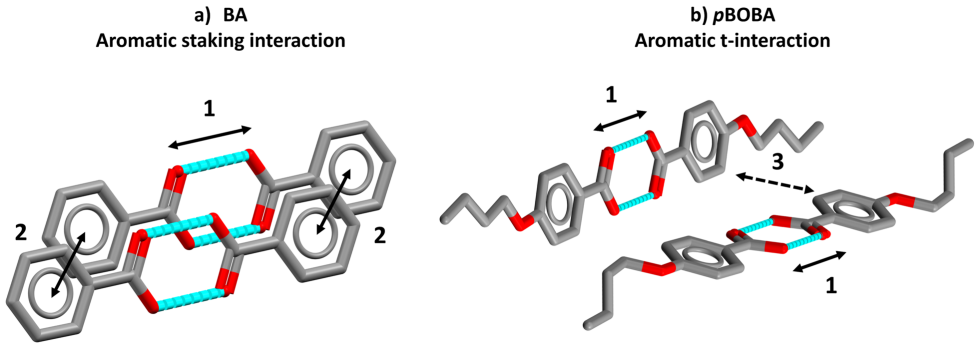

Figure 2: (a) Benzoic acid dimers (hydrogen bonded, bond 1) stacked along the b-axis (aromatic stacking interaction, bond 2). The combination of the bonds 1 and 2 is common in *p*ABA, *p*IBA, *p*BrBA and *p*NBA. These bonds are common to *p*TA as well, although the stacking involves inversion rather than translation. (b) *p*-Butoxybenzoic acid dimers (bond 1) interacting via aromatic t-type interactions (bond 3, angle between the two rings: 64.40°). Hydrogen atoms are omitted for clarity.

Prior to the nanoindentation tests, we grew good quality single crystals and indexed their dominant crystal faces (Figure 3). Figure 3(a-g) shows micrographs of a typical single crystal for each of the compounds studied and Figure 3(a'-g') displays the experimental habit together with the (hkl) values of the indented faces. Most of the compounds crystallise as needles or plates, thus exposing a limited number of dominant faces suitable for indentation. The face indexing was performed using single crystal X-Ray diffraction (XRD) which also allowed for identification of the polymorphic form (i.e. *p*ABA and *p*NBA). Since both the polymorphic form and the indentation direction can greatly affect the resulting mechanical properties measured, characterising the form and indexing the faces are crucial steps prior to indentation. Of our seven compounds, only two, *p*ABA and *p*NBA are polymorphic with the forms identified as α and II respectively. The space group data, polymorphism information and *hkl* indices for the major face for each experimental morphology are summarised in Table 1. In this study we have only indented the dominant crystal face for each of the crystals and systems. We note that Figure 3d' shows the special case of *p*ABA, which has two equally dominant faces and a square cross-section. In this case, it was thus experimentally impossible to distinguish between the (200) and (002) faces. These faces were shown to be closely related so we would not expect them to display a different mechanical behaviour.[31]

Monoclinic set: the five compounds crystallise such that the dimers (Figure 2a, via interaction 1) are oriented relative to the indentation axis at 40° (±7° among the five systems) and the aromatic stacking (Figure 2a, interaction 2) propagates parallel to the surface indented for all the 5 compounds. We recognise that there are differences between the crystal packing of the five monoclinic compounds, however the orientation relative to the indentation axis of the dimers and the aromatic stacking is retained in the five crystals.

*Triclinic set: p*TA crystal packing consists of dimers and aromatic stacking, common with the monoclinic set of compounds. However, dimers and stacking are both parallel to the indented surface, thus the dimers are oriented at 90° relative to the indentation axis instead of 40° as in the case of the monoclinic set. For the second triclinic compound *p*BOBA, the dimer (Figure 2b, interaction 1) lies at 41.3° relative to the indented surface, a very similar value to that of the monoclinic set. However, the aromatic interaction is not based on stacking but on

t-type interactions (Figure 2b, interaction 3) which creates a more complex network as discussed later.

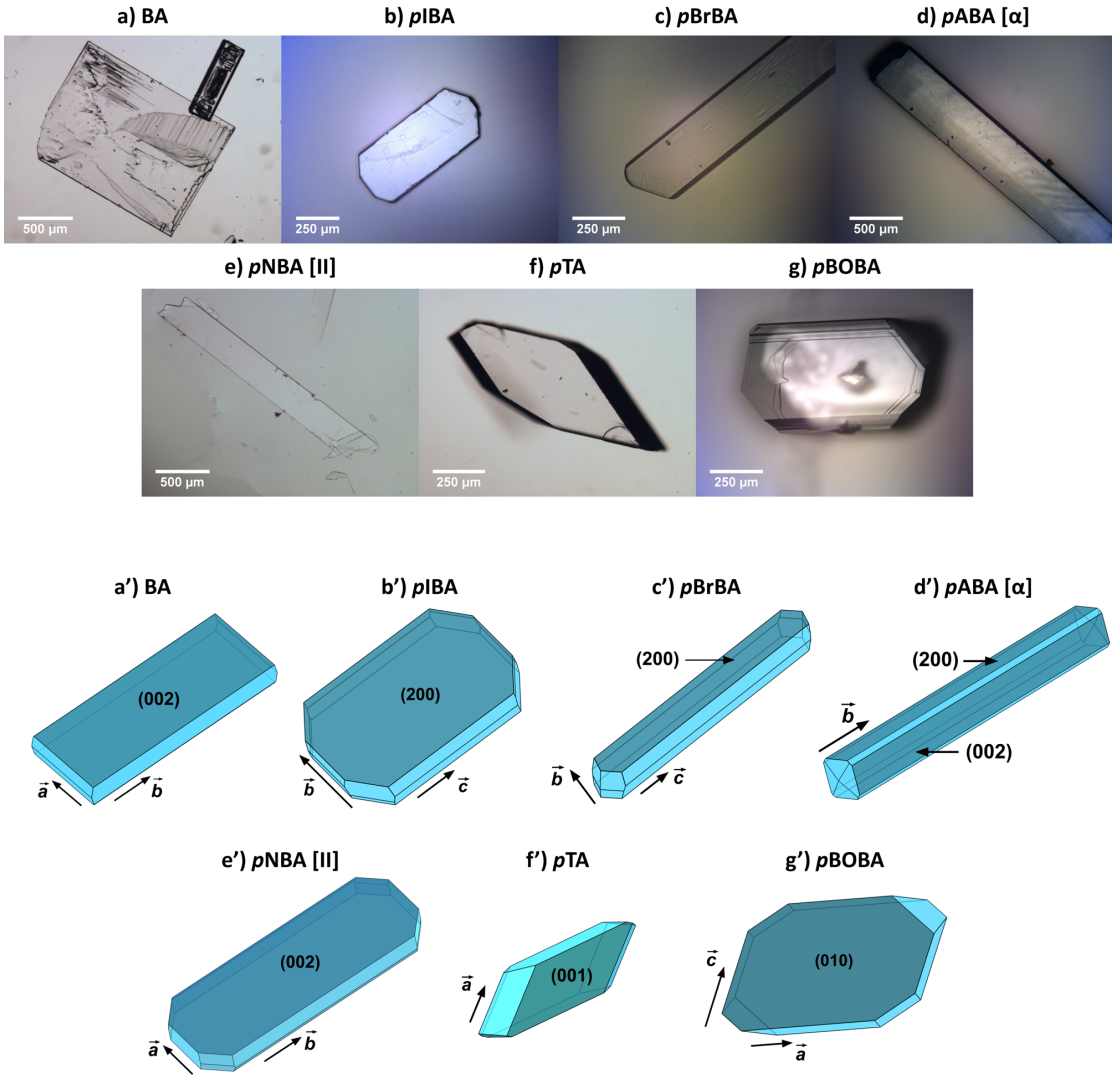

Figure 3. (a-g) Optical micrographs and (a'-g') associated face indexing of benzoic acid and every *p*-derivatives studied in this contribution.

Table 1. Summary of compounds, polymorphic forms, CSD refcodes, space group assignments and *hkl* values of their major experimental faces.

Compound	Form	CSD Refcode	Space Group	Major Face
BA	monomorphic	BENZAC02	$P2_1/c$	(002)
*p*IBA	monomorphic	BENMOW01	$P2_1/a$	(200)
*p*BrBA	monomorphic	BRBZAP	$P2_1/a$	(200)
*p*ABA	form α	AMBNAC06	$P2_1/n$	(200) / (002)
*p*NBA	form II	NBZOAC14	$P2_1/c$	(002)
*p*TA	monomorphic	PTOLIC	$P\text{-}1$	(001)
*p*BOBA	monomorphic	BUXBZA02	$P\text{-}1$	(010)

4. Results and scaling laws

a. Monoclinic systems

Nanoindentation was carried out on seven to ten single crystals for each compound using the method described in Section 3 and in more detail in our previous work.[29] Figure 4 presents a typical load - penetration curve for a single nanoindentation experiment on each single crystal from our monoclinic set, along with an in-situ scanning probe microscopy image (SPM) using the same Berkovich tip used for the indentation. The load was normalised by the maximum load in each case, P_{MAX}, to allow comparison of the curves across systems: due to abnormal variations of both E_R and H measured as previously reported,[29] the trapezoid load function used on each type of crystal was different and are presented in Electronic Supplementary Information (ESI). The mechanical results presented here are obtained for depths of penetration, h_{MAX}, at which E_R and H do not vary if h_{MAX} is further increased. BA and *p*NBA crystals tend to grow with solvent occlusions, hence they were indented in displacement-controlled mode to prevent possible drastic tip contamination, although crystals in which solvent occlusions were identified via optical microscopy were not indented. The single crystals of *p*IBA, *p*BrBA and *p*ABA were indented in load-controlled mode.

For BA only, we observe sudden and distinct displacement bursts (black arrows Figure 2b) commonly referred to as pop-ins. Pop-ins represent sudden displacements of the nanoindenter tip and this is believed to indicate the onset of dislocation motion or nucleation in the material being tested.[32] On average, only two to three pop-ins of small intensities (mostly lower than 4nm, see histogram in ESI) were clearly identified per curve. Upon indenting molecular crystals, pop-in intensities have been reported to match crystallographic data such as unit cell length or interplanar spacing, due to the gliding of crystal planes along such orientation.[21,26,33] Such correlation is hazardous because pop-ins can also be related to the presence of defects.[34] We attempted to observe this for BA but most of the pop-ins were not correlated with integers of specific d_{hkl} (presented in ESI). The curves obtained for *p*IBA, *p*BrBA, *p*ABA and *p*NBA were mostly free of pop-ins. Averages and standard deviations for E_R and H are shown in Table 2. We note that E_R and H do not necessarily increase together, with both *p*IBA and *p*BrBA having a ratio H/E_R of respectively 0.016 and 0.017, whilst this ratio increases to 0.031, 0.031 and 0.028 for BA, *p*ABA and *p*NBA respectively.

In Figure 4, the corresponding images of the indents are added to each plot. It has been shown that contact mode in-situ SPM imaging using the Berkovich tip from the indenter can damage the indent and erase features by scratching the sample surface.[29] But it was here the most appropriate imaging technique for the following reason: indents recovered quickly - sometimes within minutes - after actual indentation. Such an imaging technique allowed thus for a fast assessment of the indentation area, minimising the recovery time (lower than 3 minutes). However, imaging was still possible using ex-situ AFM on *p*ABA because it exhibited significantly slower recovery (Figure 4d). From such images, no significant pile-up of material adjacent to the indent was observed: when pile-ups were indeed observed on in-situ SPM images, for example for *p*BrBA, a pile-up formed along one indent edge only, with the height only being about 4% of the indentation contact depth. No clear crack nucleation was seen from any of the indents. This suggests plastic flow is easy within these materials.

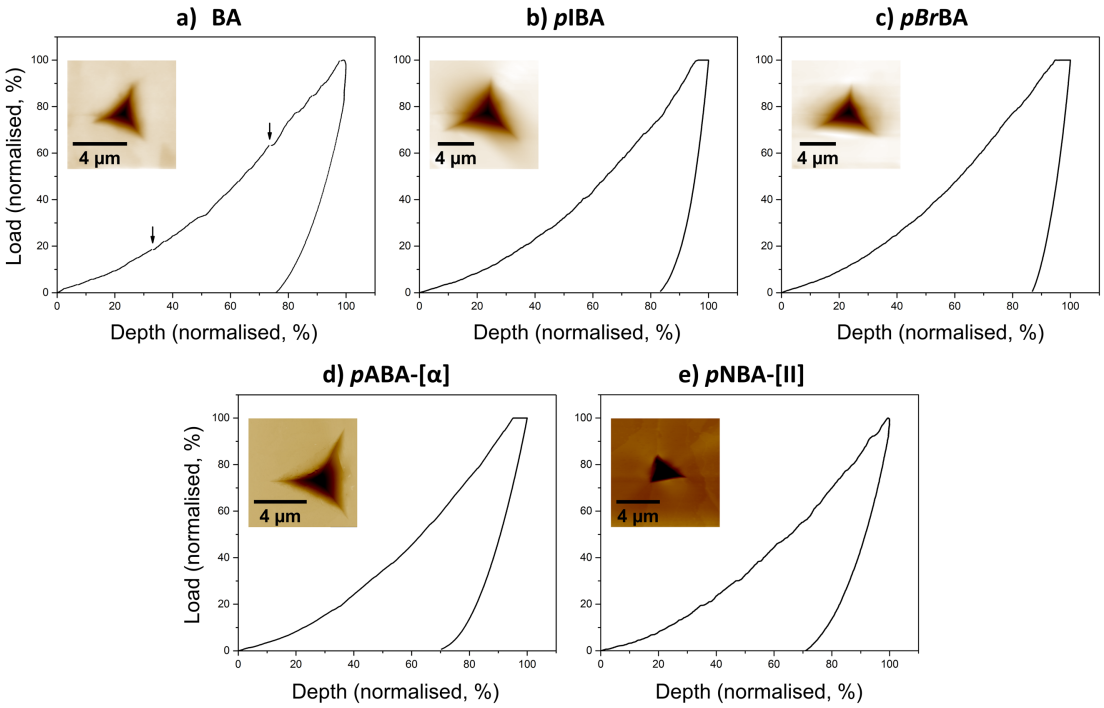

Figure 4. Typical load-depth curves obtained for each of the monoclinic crystals, presented along with their corresponding in-situ SPM imaging using the same Berkovich tip used for the indentation.

Table 2. Summary of measured E_R and H values by nanoindentation on the seven compounds studied. The experimental melting temperatures (T_M) and molecular volumes (Ω, calculated from the CSD crystal structures at room temperature) and calculated lattice energies with COMPASSII (U_{LATT}) are also given.

Crystal System	Compound	E_R ± stdv (GPa)	H ± stdv (MPa)	E ± stdv (GPa)	T_M (K)	Ω (Å^3)	U_{LATT} (kJ/mol)
Monoclinic	BA	5.22 ± 0.44	148 ± 20	4.75 ± 0.40	395.5	155	-90.1
	*p*IBA	6.46 ± 0.25	96 ± 8	5.88 ± 0.23	542.0	189	-96.9
	*p*BrBA	7.56 ± 0.47	116 ± 8	6.88 ± 0.43	529	180	-100.5
	*p*ABA [α]	7.88 ± 0.28	221 ± 17	7.17 ± 0.25	461.1	166	-104.3
	*p*NBA [II]	6.46 ± 0.28	182 ± 10	5.88 ± 0.25	513.6	176	-101.1
Triclinic	*p*TA	3.48 ± 0.35	105 ± 12	3.17 ± 0.32	453.3	180	-93.3
	*p*BOBA	4.17 ± 0.43	146 ± 12	3.79 ± 0.39	420.5	268	-117

b. Triclinic systems

Both *p*TA and *p*BOBA single crystals grew without any solvent inclusions that could be observed via optical microscopy, hence both systems were indented in the load-controlled mode. Averages and standard deviations for E_R and H are shown in Table 2 and Figure 5 presents a typical load-depth curve for a single nanoindentation experiment on each single crystal of our triclinic set, presented along with a contact mode in-situ SPM using the same Berkovich tip used for the indentation for *p*TA (Figure 5a), whilst for *p*BOBA imaging carried out via atomic force microscopy (AFM, Figure 5b) was still possible. For *p*TA,

similarly to BA as in Figure 4a, the load-depth curve shows pop-ins, however many more were observed per curve as compared to BA. In another attempt to match pop-ins intensity with crystallographic data, integers of the interplanar spacing $d(002)$ = 0.50395 nm were found to match several of the highest pop-in intensities counts centred around 6.55 nm, 7.55 nm, 8.05 nm and 8.5 nm (see histogram in ESI). However, still many pop-ins do not match this value.

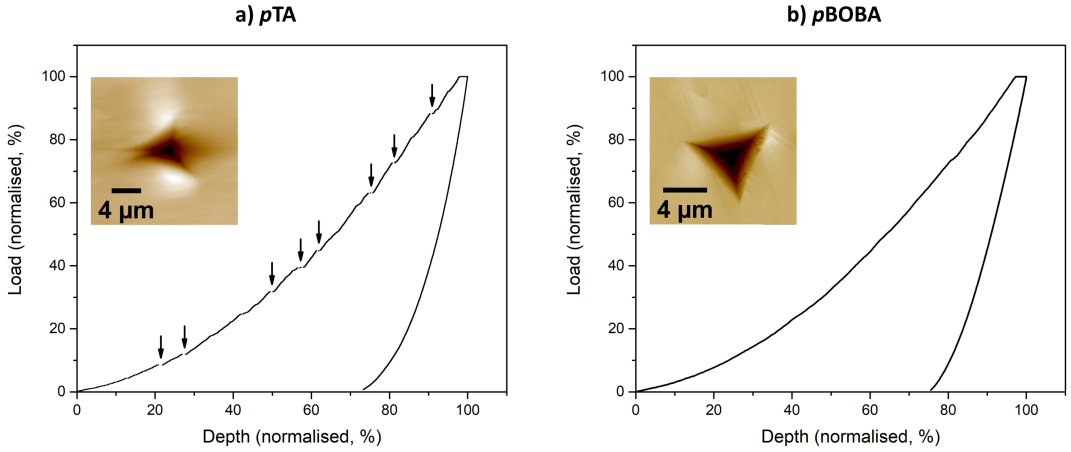

Figure 5. Typical load-depth curves obtained for the two triclinic systems, presented along with their corresponding in-situ SPM (for *p*TA, a) and atomic force microscopy imaging (AFM, for *p*BOBA, b).

c. Scaling laws

The elastic modulus and hardness measured are presented in Table 2. An assumed value of Poisson's ratio[§] was used to convert the reduced modulus to an estimated Young's modulus, also included in Table 2. In order to explore the mechanical properties correlations proposed in the literature we have also included the melting temperature of the compounds, the lattice energy, and the molecular volume at room temperature, Ω. The Young's modulus of the crystals of the seven acids are plotted against $k_B T_M/\Omega$ in Figure 6a and the best fit linear relation for six of them is shown (solid line). This line has a gradient (equal to the constant, A, in Equation 1) of approximately 489, which is somewhat larger than that proposed by Frost and Ashby for a broad range of metals and inorganic materials. In Figure 6b we show a plot of Young's modulus for all materials types using the data from Frost and Ashby's report. On this we have included our data (red circles) and data from other single-component organic molecular materials reported by Roberts et al, including aspirin, ibuprofen and sulfadiazine, amongst others.[11] Our data sits reasonably close to the trend reported by Frost and Ashby, whereas those from Roberts et al show slightly higher Young's modulus values than expected from the correlation.

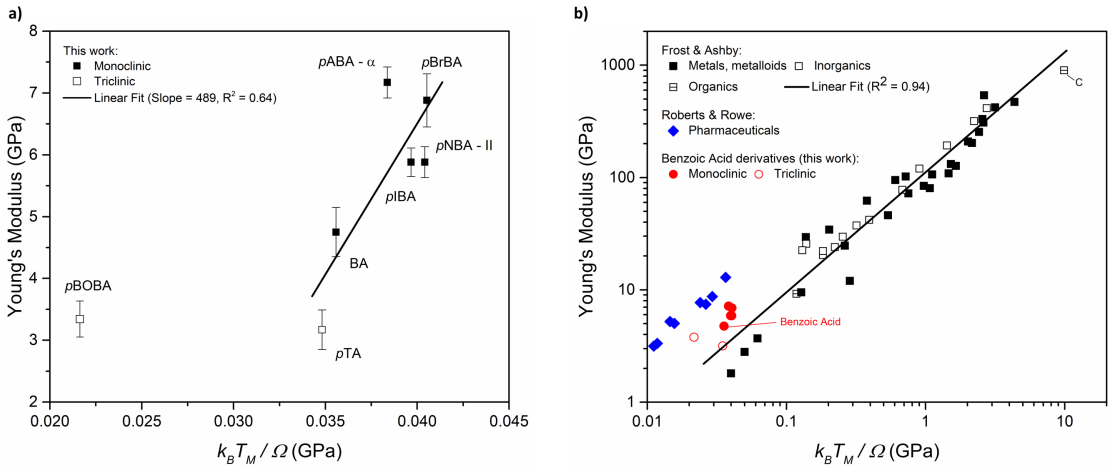

Figure 6. (a) Elastic modulus versus k_BT_M/Ω measured on the five monoclinic benzoic acid derivatives and the two triclinic (b) Elastic modulus versus k_BT_M/Ω from Roberts and Rowe's work[11] (blue diamonds), this work (red circles), and Frost and Ashby's dataset[6] of a varied set of metals and inorganic materials (black squares) logarithmically scaled.

We plot H as a function of cohesive energy density, $U_{LATT}/N_A\Omega$, (where N_A is Avogadro's number), for our data in Figure 7. We consider that the correlation using $U_{LATT}/N_A\Omega$, and k_BT_M/Ω are showing the same physical effects. It is reasonable to consider that the thermal energy of a system at its melting temperature, k_BT_M, should be positively correlated with the lattice energy.

We observe that our molecular crystal data and that from other workers show a positive deviation (larger than expected Young's modulus, see Figure 6b) from the Frost and Ashby correlation. However, the strong linear correlation between Young's modulus and k_BT_M/Ω, evident in Figure 6a supports Frost and Ashby's hypothesis, in which they indeed stated that different material groupings have different correlation constants. In which case we hypothesise that the greater deviation from the mean behaviour of Frost and Ashby's data reflects the fact that their data is predominantly from metals and ceramic materials with strong interatomic bonding. Molecular crystals have a mixture of strong intramolecular and weak intermolecular bonding suggesting a more complex relation between mechanical behaviour and melting temperature than seen with metals and ceramics. Finally, we stress that, however mechanical properties presented in Table 2 were measured at different homologous temperatures (T_{EXP} / T_M), we attempted to minimise this by using molecular volumes defined at room temperature for all the acids and U_{LATT} computed using the room temperature unit cell crystal structures.

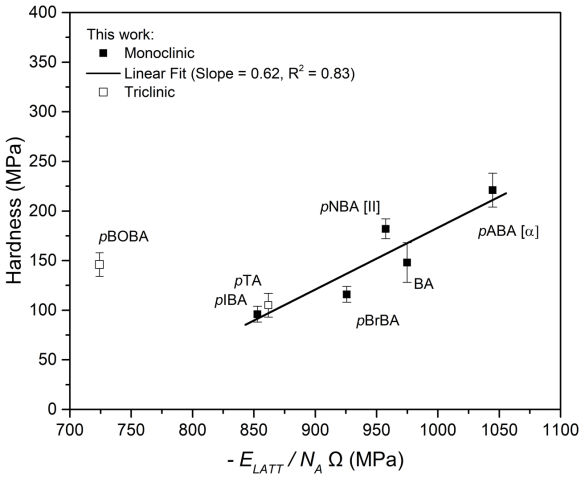

Figure 7. Hardness data obtained on 7 benzoic acid derivatives as a function of the cohesive energy density (CED).

5. Discussion

In order to understand the principles underlying the correlations between elastic modulus or hardness and lattice energy/melting point we need to consider the crystal structures of our five monoclinic crystals based on derivatives of benzoic acid as well as the two triclinic crystals. The strongest isolated intermolecular interaction in the crystals of all of these compounds is the carboxylic acid $R^2_2(8)$ dimers (cooperative hydrogen bonding). Despite being the strongest isolated interaction, however, these dimers are 0-dimensional - they do not extend in the lattice and hence do not contribute to an intermolecular hydrogen bonding network, on a longer length scale. Extended or continuous interactions (1D "chain", 2D or 3D network) that operate across the crystal lattices have been used by others to define and predict the macroscopic mechanical behaviour of crystals.[35] To aid the visualisation of the network of interactions in the crystal structures of the different acids, we calculated the Periodic Bond Chains (PBCs) in all crystal lattices using the COMPASSII forcefield as implemented in Materials Studio. PBCs, like crystal energy frameworks,[35] are a way to display the interaction network and dimensionality of molecule-molecule interactions in crystals. All molecule-molecule interactions are calculated, and lines are drawn from the centroid of a molecule to the centroid of the interacting molecule with different colours (strengths, blue stronger than red). A cuf-off energy is applied (-13 kJ/mol in our case) thus only the main molecule-molecule interactions (usually molecule-molecule interactions dominated by hydrogen bonds and aromatic stacks in our case[31]) are displayed and a network is revealed upon displaying a number of unit cells (Figure 8). Perhaps fortuitously, we found that the orientation of the PBCs with respect to the indentation axis and the PBC networks were very similar for all crystals of the acids studied with the exception of *p*BOBA (different PBCs) and *p*TA (different orientation of PBCs with respect to the indentation direction).

In Figure 8 the PBCs of BA and *p*BOBA are displayed and viewed along their three crystallographic axes (see ESI for *p*TA and the other acids). In the BA crystal structure (and similarly in the structures of *p*IBA, *p*ABA, *p*NBA and pBrBA) each BA acid is involved in three significant molecule-molecule interactions: a hydrogen bonded dimer interaction via the –COOH group (-54 kJ/mol) and two aromatic stacking interactions through translation (+b,-b) along the b-axis of around -13 kJ/mol each. The weak but continuous aromatic stacking along

the b-axis generates the 1D PBC in the BA crystal structure (linear structure). In the *p*TA crystal structure, each molecule is also involved in three significant molecule-molecule interactions: a hydrogen bonded dimer interaction via the –COOH group and two aromatic stacking interactions related by inversion of around -20 kJ/mol each. A 2D PBC is generated in the *p*TA crystal structure (layered structure), instead of a 1D structure because the stacking interactions are related by inversion and the HB dimers are shifted relative to each other. In the *p*BOBA crystal structure, each molecule is involved in four significant molecule-molecule interactions: a hydrogen bonded dimer interaction via the –COOH group and three aromatic t-type of interactions of ~ -26 kJ/mol each. In this case the hydrogen-bonded dimers are shifted relative to each other (Figure 8, a'-c'), hence they also contribute significantly to the generation of the 3D PBCs which run along all three crystal directions (3D-network structure), mainly due to a combination of three medium strength t-type interactions and the HB dimers (see Figure 2).

This structural analysis suggests that both 1D and 2D PBCs may allow for the plastic deformation throughout the slip of specific planes bonded together via weaker interactions (planes that do not break the PBCs). Interestingly, we found that the active slip planes do not necessarily need to be perpendicular to the indented face. This is the case of *p*TA whose 2D-PBC layers stack along the indentation direction. Perhaps as a consequence of that, whilst we cannot image the slips because of fast recovery after indentation, we observe a significant number of pop-ins as the layers break upon nanoindentation. Despite the 2D-layers stacking along the indentation direction, the material is still very soft. This is because a Berkovich tip does not create a unique stress field parallel to the indentation axis but rather a half spherical stress distribution.

Similar rationalisations of brittleness, plasticity or bending behaviour in molecular crystal have been presented by Turner et al. with the aid of energy frameworks (analogous to PBCs).[35] Our work constitutes a good experimental application of theirs, highlighting that the dimensionality of PBCs is key in the mechanical overall behaviour of similar compounds. And in our particular case, it highlights the role of softer aromatic interactions in shaping mechanical behaviour. The stronger and also higher dimensionality of interactions in *p*BOBA crystals makes the material behave very differently to the rest of the acids, which have either 1D or 2D dimensionality and clear slip planes.

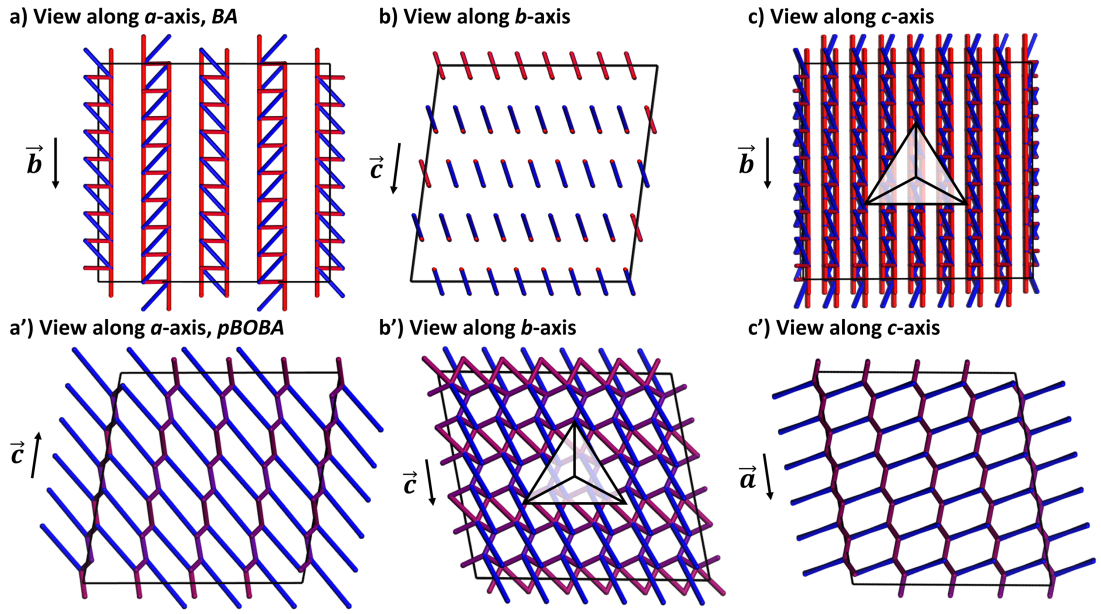

Figure 8. Computed PBCs for the crystal structures of (a-c) BA (BENZAC02) and (a'-c') *p*BOBA (BUXBZA02) viewed along their three principal axes. Only interactions more stabilising than -13 kJ/mol are displayed. In this system, blue tubes represent molecule-molecule interactions dominated by hydrogen bonds (around -54 kJ/mol) and red tubes represent molecule-molecule interactions dominated by aromatic stacking (BA, -13 kJ/mol) and purple tubes represent molecule-molecule interactions dominated by aromatic t-interactions (*p*BOBA, ~ -26 kJ/mol). The indentation orientation is indicated via the equilateral triangle (c and b'). PBCs are analogous to crystal energy frameworks and can be interpreted in the same way: discrete lines (blue lines) are 0 dimensional interactions, continuous lines are 1 dimensional interactions (red and purple lines), and the assembly of different lines can result in higher dimensionality interactions network.[35]

Given our analysis, it appears that the Frost and Ashby's and Roberts and Rowe's correlations hold for isomechanical groups in molecular crystals. The key challenge thus is to identify which crystals of which compounds belong to similar isomechanical groups. We have shown even for a series of similar compounds that these will not all belong to the same isomechanical groups. Polymorphs, for example, do not necessarily belong to the same group either: a recent review by C. Sun points out that the comparison of mechanical properties *E* and *H* between polymorphs of the same compound lead to a ratio Highest/lowest Young's modulus (and hardness) between two polymorphs that can be as high as 3 (2.5 times for the hardness).[23] Different polymorphs usually possess slightly different mean molecular volumes, but this cannot explain such a high a ratio of 3 or 2.5 times. Changes in the intermolecular interactions and crystal structure in polymorphs together with a change in the available crystal faces for indentation (mechanical properties are strongly dependent on the crystal direction) must thus account for such large differences.

An analysis of the crystal structures and intermolecular interactions present in these crystals allowed for some rationalisation as to why *p*BOBA does not seem to belong to the same isomechanical group as the rest of the benzoic acids. Unlike the rest of the acids whose crystal structures are built on 1D and 2D interaction networks, *p*BOBA is more tightly bound in a 3D network of PBCs. This results in the *p*BOBA crystals being much harder than what it would have been predicted based on the correlations derived for the rest of the acids. The novelty of this observation is that whilst the impact of interaction dimensionality in crystals' mechanical properties has mostly been highlighted for hydrogen bond networks[36], the 3D PBCs in the *p*BOBA lattice rely on a combination of hydrogen bonds and aromatic interactions, in this case of t-type. Whilst aromatic stacking can only allow for 1D PBCs (only

two stacking interactions are possible per ring), t-type of interactions can allow for 2D PBCs (each ring can be involved in four t-type of interactions). This reveals how important the cumulative effect and the dimensionality of weak/medium interactions is in the mechanical response of these molecular materials.

6. Conclusion

Nanoindentation has been used to measure the elastic modulus and hardness of crystal faces in a series of benzoic acid derivatives that crystallise in monoclinic or triclinic systems. These mechanical properties have been compared with literature data of other molecular crystals. Semi-empirical scaling laws, established previously for polycrystalline metals, were successfully applied to correlate Young's modulus and hardness with physical properties of these benzoic acid derivatives crystals that are either easily measured (melting point) or easily computed (cohesive energy densities).

From the analysis and comparisons of the nanoindentation results, it was shown that the *p*-butoxy derivative of benzoic acid was surprisingly stiff and hard despite the compound being a larger molecule, with a low melting point and comparatively low cohesive energy density. Such deviation was rationalised via the analysis of the intermolecular interactions throughout our set of compounds. The analysis revealed that, although often overlooked, aromatic interactions play a key role in the mechanical response of these molecular materials. Revealingly, whilst aromatic stacking only expands in one-direction, aromatic t-type of interactions can expand in at least two, which is more likely to generate harder materials.

Given these findings, it would be useful to apply the concept of isomechanical groups for similar compounds with lattices consisting of similar intermolecular interactions. This would enable the derivation of empirical models for the prediction of mechanical properties of other compounds also belonging to the same group. Given how common it is for the pharmaceutical industry to develop a series of similar derivatives to be tested as drugs, the development of *isomechanical groups* with these similar derivatives may be useful and enable the prediction of hardness and elasticity within series of drug candidates.

7. Associated Content

Supporting Information

The Supporting Information is available free of charge via the Internet at http://pubs.acs.org.

Load-functions used in the nanoindentation experiments, DSC results, analysis of pop-ins for BA and *p*TA, Periodic Bond Chains for all seven systems.

Acknowledgements

BG thanks Roche and the University of Manchester for financial support, Sin Kim Tang for her help crystallising *p*TA and *p*BOBA crystals, and the staff in the Department of Chemistry XRD Facility in the School of Natural Sciences at the University of Manchester for their assistance. AJCC thanks the Royal Society for an industry Fellowship in AstraZeneca. This work was supported by the Henry Royce Institute for Advanced Materials, funded through EPSRC grants EP/S009493/1, EP/R00661X/1, EP/P025021/1 and EP/P025498/1. The authors thank Dr Pirmin Hidber for helpful discussions.

Footnotes and references

§ We note that the Young's modulus (E) can be calculated from the measured reduced modulus (E_R) using the Poisson coefficient ν typical for these materials. We do not have these coefficients readily available for each material, however they were assumed here to be all ν = 0.3, reported in the literature for organic molecular materials as typical values.

(1) Kalaria, D. R.; Parker, K.; Reynolds, G. K.; Laru, J. An Industrial Approach towards Solid Dosage Development for First-in-Human Studies: Application of Predictive Science and Lean Principles. *Drug Discov. Today* **2020**, *25*, 505–518.

(2) Beaman, R. G. Relation between (Apparent) Second-Order Transition Temperature and Melting Point. *J. Polym. Sci.* **1952**, *9*, 470–472.

(3) Brown, A. M.; Ashby, M. F. Correlations for Diffusion Constants. *Acta Metall.* **1980**, *28*, 1085–1101.

(4) Ashby, M. F. Checks and Estimates for Material Properties I. Ranges and Simple Correlations. *Proc. R. Soc. A Math. Phys. Eng. Sci.* **1998**, *454*, 1301–1321.

(5) Bassetti, D.; Brechet, Y.; Ashby, M. F. Estimates for Material Properties II. the Method of Multiple Correlations. *Proc. R. Soc. A Math. Phys. Eng. Sci.* **1998**, *454*, 1323–1336.

(6) Frost, H. J.; Ashby, M. F. Scaling Laws and Isomechanical Groups. In *Deformation-mechanism Maps: The Plasticity and Creep of Metals and Ceramics*; 1982; pp 133–140.

(7) Sammis, C. G.; Smith, J. C.; Schubert, G. A Critical Assessment of Estimation Methods for Activation Volume. *J. Geophys. Res. Solid Earth* **1981**, *86*, 10707–10718.

(8) Derby, B. Correlations for Single-Crystal Elastic Constants of Compound Semiconductors and Their Representation in Isomechanical Groups. *Phys. Rev. B - Condens. Matter Mater. Phys.* **2007**, *76*, 1–12.

(9) Plummer, J. D.; Todd, I. Isomechanical Groups in Bulk Metallic Glasses. *Philos. Mag.* **2012**, *92*, 2894–2910.

(10) Roberts, R. J.; Rowe, R. C.; York, P. The Relationship between Indentation Hardness of Organic Solids and Their Molecular Structure. *J. Mater. Sci.* **1994**, *29*, 2289–2296.

(11) Roberts, R. J.; Rowe, R. C.; York, P. The Relationship between Young's Modulus of Elasticity of Organic Solids and Their Molecular Structure. *Powder Technol.* **1991**, *65*, 139–146.

(12) Feld, R.; Lehmann, M. S.; Muir, K. W.; Speakman, J. C. The Crystal Structure of Benzoic Acid: A Redetermination with X-Rays at Room Temperature; a Summary of Neutron-Diffraction Work at Temperatures down to 5 K. *Zeitschrift für Krist. - Cryst. Mater.* **1981**, *157*, 215–231.

(13) Takwale, M. G.; Pant, L. M. The Structure of P-Toluic Acid. *Acta Crystallogr. Sect. B Struct. Crystallogr. Cryst. Chem.* **1971**, *27*, 1152–1158.

(14) Athimoolam, S.; Natarajan, S. 4-Carboxy-Anilinium (2R,3R)-Tartrate and a Redetermination of the α-Polymorph of 4-Amino-Benzoic Acid. *Acta Crystallogr. Sect. C Cryst. Struct. Commun.* **2007**, *63*, 514–517.

(15) Light, M. E. CCDC 1476879. *CSD Commun.* **2016**.

(16) Ohkura, K.; Kashino, S.; Haisa, M. The Crystal and Molecular Structure of P-Bromobenzoic Acid. *Bull. Chem. Soc. Jpn.* **1972**, *45*, 2651–2652.

(17) Baughman, R. G.; Nelson, J. E.; IUCr. The Structure of P-Iodobenzoic Acid, C7H5IO2. *Acta Crystallogr. Sect. C Cryst. Struct. Commun.* **1984**, *40*, 204–206.

(18) Kuz'mina, L. G.; Kucherepa, N. S.; Pestov, S. M.; Kochetov, A. N.; Rukk, N. S.; Syrby, S. A. Molecular and Crystal Structure of 4-Alkoxybenzoic Acids: Design of the Mesogenic Phase. *Kristallografiya* **2009**, *54*, 908–925.

(19) Oliver, W. C.; Pharr, G. M. An Improved Technique for Determining Hardness and Elastic Modulus Using Load and Displacement Sensing Indentation Experiments. *J. Mater. Res.* **1992**, *7*, 1564–1583.

(20) Oliver, W. C.; Pharr, G. M. Measurement of Hardness and Elastic Modulus by Instrumented Indentation: Advances in Understanding and Refinements to Methodology. *J. Mater. Res.* **2004**, *19*, 3–20.

(21) Kiran, M. S. R. N.; Varughese, S.; Reddy, C. M.; Ramamurty, U.; Desiraju, G. R. Mechanical Anisotropy in Crystalline Saccharin: Nanoindentation Studies. *Cryst. Growth Des.* **2010**, *10*, 4650–4655.

(22) Ramamurty, U.; Jang, J. Il. Nanoindentation for Probing the Mechanical Behavior of Molecular Crystals-a Review of the Technique and How to Use It. *CrystEngComm* **2014**, *16*, 12–23.

(23) Wang, C.; Sun, C. C. The Landscape of Mechanical Properties of Molecular Crystals. *CrystEngComm* **2020**, *20*, 1149–1153.

(24) ISO 14577:2015, "Metallic Materials — Instrumented Indentation Test for Hardness and Materials Parameters." *Int. Organ. Stand. Geneva, Switz.*

(25) Ramos, K. J.; Bahr, D. F. Mechanical Behavior Assessment of Sucrose Using Nanoindentation. *J. Mater. Res.* **2007**, *22*, 2037–2045.

(26) Varughese, S.; Kiran, M. S. R. N.; Solanko, K. A.; Bond, A. D.; Ramamurty, U.; Desiraju, G. R. Interaction Anisotropy and Shear Instability of Aspirin Polymorphs Established by Nanoindentation. *Chem. Sci.* **2011**, *2*, 2236–2242.

(27) Lubomirsky, I.; Azuri, I.; Meirzadeh, E.; Ehre, D.; Cohen, S. R.; Rappe, A. M.; Lahav, M.; Kronik, L. Unusually Large Young's Moduli of Amino Acid Molecular Crystals. *Angew. Chemie - Int. Ed.* **2015**, *54*, 13566–13570.

(28) CrysAlis PRO, Version 171.40.14d, Oxford Diffraction /Agilent Technologies UK Ltd, Yarnton,

England. 2018.
(29) Gabriele, B. P. A.; Williams, C. J.; Lauer, M. E.; Derby, B.; Cruz-Cabeza, A. J. Nanoindentation of Molecular Crystals: Lessons Learned from Aspirin. *Cryst. Growth Des.* **2020**, *20*, 5956–5966.
(30) Dassault Systèmes BIOVIA, Materials Studio, Release 2019, San Diego: Dassault Systèmes. 2019.
(31) Cruz-Cabeza, A. J.; Davey, R. J.; Sachitananthan, S. S.; Smith, R.; Tang, S. K.; Vetter, T.; Xiao, Y. Supporting Information for: "Aromatic Stacking - a Key Step in Nucleation." **2017**, 1–22.
(32) Lorenz, D.; Zeckzer, A.; Hilpert, U.; Grau, P.; Johansen, H.; Leipner, H. S. Pop-in Effect as Homogeneous Nucleation of Dislocations during Nanoindentation. *Phys. Rev. B - Condens. Matter Mater. Phys.* **2003**, *67*, 1–4.
(33) Mishra, M. K.; Ramamurty, U.; Desiraju, G. R. Solid Solution Hardening of Molecular Crystals: Tautomeric Polymorphs of Omeprazole. *J. Am. Chem. Soc.* **2015**, *137*, 1794–1797.
(34) Liu, F.; Hooks, D. E.; Li, N.; Rubinson, J. F.; Wacker, J. N.; Swift, J. A. Molecular Crystal Mechanical Properties Altered via Dopant Inclusion. *Chem. Mater.* **2020**, *32*, 3952–3959.
(35) Turner, M. J.; Thomas, S. P.; Shi, M. W.; Jayatilaka, D.; Spackman, M. A. Energy Frameworks: Insights into Interaction Anisotropy and the Mechanical Properties of Molecular Crystals. *Chem. Commun.* **2015**, *51*, 3735–3738.
(36) Bryant, M. J.; Maloney, A. G. P.; Sykes, R. A. Predicting Mechanical Properties of Crystalline Materials through Topological Analysis. *CrystEngComm* **2018**, *20*, 2698–2704.

For Table of Contents Use Only

Isomechanical Groups in Molecular Crystals and Role of Aromatic Interactions

Benjamin P. A. Gabriele[a], Craig J. Williams[b], Matthias Eckhard Lauer[c], Brian Derby[b], Aurora J. Cruz-Cabeza[a]*

TOC Graphic

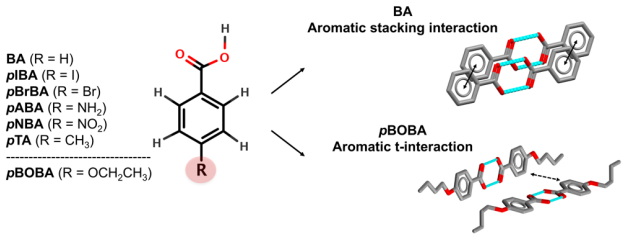

Synopsis

We correlate mechanical properties measured in molecular crystals of a series of para-substituted benzoic acids, first with their melting point per unit of volume and second with the crystals' cohesive energy density. Structures with aromatic rings interacting through t-type interactions may achieve higher interaction dimensionalities and thus result in harder crystals than those with rings interacting through aromatic stacking.